Available online at www.sciencedirect.com
SCIENCE DIRECT®
Journal of Power Sources 117 (2003) 61–74
JOURNAL OF POWER SOURCES
www.elsevier.com/locate/jpowsour

A general mathematical model for analyzing the performance of fuel-cell membrane-electrode assemblies

Huayang Zhu*, Robert J. Kee

Engineering Division, Colorado School of Mines, Golden, CO 80401, USA

Received 9 January 2003; accepted 27 January 2003

Abstract

We have developed a general mathematical model to represent the membrane-electrode assembly (MEA) of fuel-cell systems. The model is used to analyze the effects of various polarization resistances on cell performance. The model accommodates arbitrary gas mixtures on the anode and cathode sides of the MEA. Moreover, it accommodates a variety of porous electrode and electrolyte structures. Concentration overpotentials are based on a dusty-gas representation of transport through porous electrodes. The activation overpotentials are represented using the Butler–Volmer equation. Although the model is general, the emphasis in this paper is on solid-oxide fuel-cell (SOFC) systems for the direct electrochemical oxidation (DECO) of hydrocarbons.

Keywords: Model; MEA; Fuel cell; SOFC

1. Introduction

Quantitative models can be valuable in the interpretation of experimental observations and in the development and optimization of systems. The objective of the membrane-electrode assembly (MEA) model developed herein is to provide a physically based model that can be used to evaluate the effects of design and operating alternatives. While the model can stand alone, the software is written in a way that enables incorporation into larger system-level models that also consider fluid flow and thermal management throughout a fuel-cell system. The model is general in the sense that it can accommodate a variety of geometrical configurations. It can also represent proton-conducting or oxygen-ion-conducting electrolytes. The discussion and examples in this paper, however, consider solid-oxide fuel-cell (SOFC) system.

The great advantage of SOFC systems for highly efficient electric power generation lies in its potential for direct use of hydrocarbon fuels, without the requirement for upstream fuel preparation, such as reforming [1–4]. A typical layout for a planar design of the SOFC system is illustrated in Fig. 1. The membrane-electrode assembly, which is composed of an electrolyte sandwiched between the anode and the cathode, is itself sandwiched between metal interconnect structures. The fuel and air channels are formed in the interconnect structure. The electrolyte is a dense ceramic (e.g. yttria-stabilized zirconia (YSZ) or gadolinia-doped ceria (GDC)), which is impermeable to gas flow but is an oxygen-ion (O^{2-}) conductor. The composite electrodes are porous metal-loaded ceramics (cermets) (e.g. Ni–YSZ for the anode and Sr-doped $LaMnO_3$ (LSM) for the cathode), which may be mixed electronic and ionic conductors that can extend the three-phase boundaries (TPB) and promote the electrocatalytic reactions.

The SOFC system involves complex transport, chemical, and electrochemical processes, with its operating performance strongly affected by the corresponding transport resistances and the activation barriers. Fig. 2 illustrates some of these processes at the MEA level. During operation, oxygen from the air channel transports through the porous cathode, whereupon it is reduced to oxygen ion (O^{2-}) at gas–cathode–electrolyte three-phase boundaries. The formed oxygen ion at the cathode–electrolyte interface is then transported to the anode–electrolyte interface through the ion-conducting electrolyte. At the same time, fuel from the fuel channel transports through the porous anode to the anode–electrolyte interface, where it is oxidized electrochemically at the gas–anode–electrolyte three-phase boundaries to products. The products (e.g. H_2O and CO_2) are then transported back to the fuel channel through the porous anode structure. Transport resistances of the gas-phase species in the porous electrodes and O^{2-} in the electrolyte,

* Corresponding author. Tel.: +1-303-273-3890; fax: +1-303-273-3602.
E-mail address: hzhu@mines.edu (H. Zhu).

0378-7753/03/$ – see front matter © 2003 Elsevier Science B.V. All rights reserved.
doi:10.1016/S0378-7753(03)00358-6

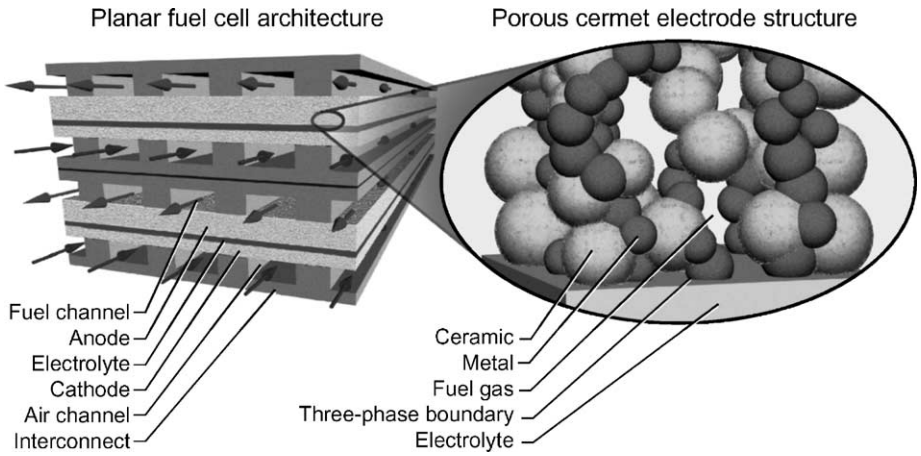

Fig. 1. Typical layout of a planar SOFC. The left-hand panel illustrates the system at the scale of flow channels (in mm), while the right-hand panel illustrates the small-scale structure (in μm) of the porous cermet electrode.

as well as the activation energy barriers for electrochemical reactions can result in various polarizations. They are represented as concentration overpotentials, activation overpotentials, and ohmic overpotentials. The main contribution to the ohmic polarization is from the transport resistance of O^{2-} in the electrolyte. The concentration polarization is due to the transport resistance of the gaseous species through porous composite electrodes, and the activation polarization is related to the charge-transfer processes at the electrode–electrolyte interfaces. These various polarizations are functions of both operating conditions and the physical properties of the cell. The operating conditions include temperature, pressure, and fuel and oxidizer concentrations. The cell properties involve materials, macro- and microstructures of the electrolyte and the composite electrodes, which include porosity, tortuosity, permeability, and thickness of the anode and the cathode, the ionic conductivity and thickness of the electrolyte, the active area and activity of the electrode–electrolyte interface.

To understand these various resistances and enhance the cell performance, parametric studies for these various polarizations in the electrolyte and composite electrodes have been widely made through experiments [5,6], theoretical analysis [7], and numerical models [8–10]. The theoretical analyses and numerical models for the activation polarizations require an understanding the elementary thermal–electrochemical reaction mechanisms and the microstructure of the electrode. Due to the complex and uncertain details of the reaction processes (particularly in case of hydrocarbons), most modeling in the literature has focused on using H_2 as the fuel. Chan et al. [8] used the intrinsic charge-transfer resistance to represent the activation polarization. Tanner et al. [11] have derived an effective charge-transfer resistance for the composite electrode, which is a function of the microstructural parameters of the electrode, intrinsic charge-transfer resistance, ionic conductivity of the electrolyte, and the electrode thickness. This effective charge-transfer resistance model was later used to analyze the activation overpotentials [9,10]. Adler et al. [12] derived a charge-transfer resistance model for the composite cathode, which is a function of the tortuosity, porosity, interface area, oxygen self-diffusion coefficient and oxygen exchange coefficient. The activation polarizations for a particular electrode may also be measured by the electrochemical impedance spectroscopy (EIS) [5,6,13]. Previous porous-media gas-phase transport models have been developed to predict concentration overpotentials [8–10]. These include molecular diffusion, Knudsen diffusion, and pressure-driven Darcy flow. However, these have only been applied in fuel-cell systems with binary gas-phase mixtures.

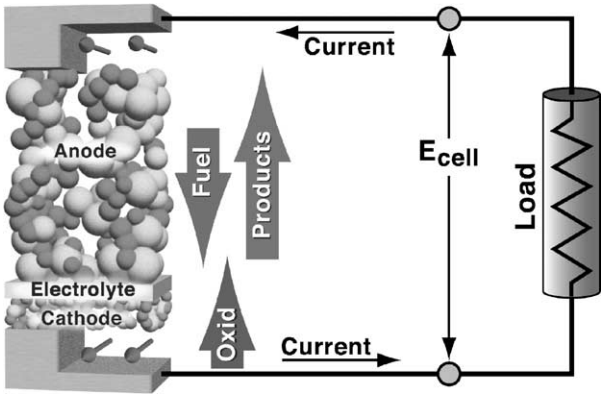

Fig. 2. Illustration of the components of the MEA unit cell.

The model developed in this paper represents a unit-cell structure (Fig. 2), considering the effects of various overpotentials on the cell performance. As illustrated in Fig. 2 the cell is anode-supported, with a very thin electrolyte and cathode, and both electrodes are porous ceramic–metal composite structures. Channels formed in an interconnect structure carry the flow of fuel and air. Depending on the position of the unit cell within a fuel-cell system, the composition in both the fuel and air channels varies depending on initial composition and depletion.

2. Model formulation

The overall performance of SOFC systems is greatly affected by ohmic, concentration, and activation polarizations. Thus, the operating cell potential (E_{cell}) is lower than the Nernst potential (E). The operating cell potential (E_{cell}) can be formally expressed as:

$$E_{\text{cell}} = E - \eta_{\text{conc,a}} - \eta_{\text{act,a}} - \eta_{\text{ohm}} - \eta_{\text{conc,c}} - \eta_{\text{act,c}} - \eta_{\text{interface}} - \eta_{\text{leakage}}, \quad (1)$$

where $\eta_{\text{conc,a}}$ and $\eta_{\text{conc,c}}$ are the concentration overpotentials at the anode and the cathode due to the gas-phase species diffusion resistance, $\eta_{\text{act,a}}$ and $\eta_{\text{act,c}}$ the corresponding activation overpotentials, η_{ohm} the ohmic overpotential in the electrolyte, $\eta_{\text{interface}}$ the interface overpotential due to the contact resistance at material boundaries, and η_{leakage} the cell potential loss due to the electric current through the electrolyte. Subsequent sections in the paper develop models for each of these overpotentials, all of which are functions of the current density i_{e}.

2.1. Global electrochemical reaction

A global electrochemical reaction can be written as:

$$\nu_{\text{f}}'\left(\sum_{k=1}^{K} n_{\text{f},k}\chi_k\right) + \nu_{\text{o}}'\left(\sum_{k=1}^{K} n_{\text{o},k}\chi_k\right) \leftrightarrows \sum_{k=1}^{K} \nu_{\text{f},k}''\chi_k + \sum_{k=1}^{K} \nu_{\text{o},k}''\chi_k, \quad (2)$$

where χ_k is the chemical symbol for the kth species (which may participate as a fuel, an oxidizer, or both), ν_{f}' and ν_{o}' the stoichiometric coefficients for the fuel and oxidizer mixtures, and $\nu_{\text{f},k}''$ and $\nu_{\text{o},k}''$ the stoichiometric coefficients of the kth product species in the fuel and air channels, respectively. Each species χ_k has a primary identity as a fuel, an oxidizer, a product, or an inert, and this identity plays an essential role in balancing the reaction to determine stoichiometric coefficients and in assigning charge transfer. The global reaction can be expressed in compact form as:

$$\sum_{k=1}^{K} \nu_k'\chi_k \leftrightarrows \sum_{k=1}^{K} \nu_k''\chi_k, \quad (3)$$

where $\nu_k' = \nu_{\text{f}}' n_{\text{f},k} + \nu_{\text{o}}' n_{\text{o},k}$ and $\nu_k'' = \nu_{\text{f},k}'' + \nu_{\text{o},k}''$.

Fuel and oxidizer mixtures are separated by the anode–electrolyte–cathode MEA structure. Thus, in writing a global electrochemical reaction and calculating the Nernst potential, it is convenient to represent the fuel mixture and the oxidizer mixture separately as reactants. This separation is accomplished by writing the LHS of the reaction as two summations. The fuel channel mixture composition is represented in terms of the species mole numbers as $n_{\text{f},k}$. Similarly, $n_{\text{o},k}$ is used to represent the mixture of the composition of the oxidizer mixture in the air channel (e.g. for air, $n_{\text{o,O}_2} = 0.21$ and $n_{\text{o,N}_2} = 0.79$).

The RHS of the global reaction is also separated into two terms. Depending on whether the cell is an oxygen-ion conductor or a proton conductor, the product species appear on the anode or cathode side of the MEA. Thus, following reaction balancing, the location of the product species affects the product stoichiometric coefficients $\nu_{\text{f},k}''$ and $\nu_{\text{o},k}''$. There is more discussion on this point following the discussion on reaction balancing.

Since the electrochemical reactions involve charge transfer it is necessary to specify the charge transfer associated with each *reactant* species. For this purpose, we introduce two sets of parameters ($z_{\text{f},k}$ and $z_{\text{o},k}$), which specify the charge transferred per mole of the kth fuel and oxidizer species. For a species that is inert relative to the electrochemical charge-transfer process, $z = 0$. In our convention, the product species (e.g. H_2O and CO_2) also are assigned $z = 0$. Consider two examples for assigning z. Since O_2 in the air channel is reduced to O^{2-} by obtaining four electrons (i.e. $O_2 + 4e^- \rightarrow 2O^{2-}$), the parameter $z_{\text{o,O}_2} = 4$. Because the direct electrochemical reaction of CH_4 with O^{2-} at the anode to produce H_2O and CO_2 (i.e. $CH_4 + 4O^{2-} \rightarrow CO_2 + 2H_2O + 8e^-$) releases eight electrons, $z_{\text{f,CH}_4} = 8$. The total number of electrons transferred by the global electrochemical reaction is represented as:

$$n_{\text{e}} = \sum_{k=1}^{K} \nu_{\text{f}}' n_{\text{f},k} z_{\text{f},k} = \sum_{k=1}^{K} \nu_{\text{o}}' n_{\text{o},k} z_{\text{o},k}. \quad (4)$$

There may be reasons to incorporate oxidizer species into the fuel channel or fuel species into the oxidizer channel. For example, oxygen in the fuel channel may promote beneficial partial oxidation of the fuel or it may work to inhibit deposit formation. Such species, while influencing thermal chemistry in the gas or on catalytic surfaces, do not participate directly in the electrochemical reaction. Thus, they are considered inert in the global electrochemical reaction. For example, if O_2 (i.e. an oxidizer species) appears as part of the fuel composition (i.e. in the first term of the global reaction (2)), then $z_{\text{f,O}_2} = 0$. The added oxygen in the fuel channel cannot work directly to produce electric energy—only fuel oxidization with oxidizer from the cathode channel can produce power. Thus, any oxidizer in the fuel channel must reduce the cell potential because of its diluting effect.

Before proceeding to evaluate the cell potential, the global reaction must be balanced to determine the stoichiometric coefficients. Although balancing reactions is a well known process, a few words of explanation are warranted. A balance equation is written for each element (e.g. H, C, O, N), requiring that the reaction conserves the element balance. The process leads to a system of linear equations for the stoichiometric coefficients (ν_{f}', ν_{o}', and ν_k''). Because of an essential linear dependence stemming from the fact that species are composed of elements in a specified way, one can arbitrarily set $\nu_{\text{f}}' = 1$. Then depending on the number of product species, only some of the ν_k'' are non-trivial. Specifically, the number of product species (and hence the

number v_k'' coefficients) is one fewer than the number of elements. Once the overall product stoichiometric coefficients v_k'' are known, then either:

$$v_{f,k}'' = v_k'' \quad \text{or} \quad v_{o,k}'' = v_k'', \tag{5}$$

depending on the type of cell (i.e. oxygen ion or proton conducting) and hence the location of the product species.

Inert species (i.e. *reactant* species for which $z_{f,k} = 0$ and $z_{o,k} = 0$) are initially excluded from the balancing procedure. Once the balance is completed, the inert species are reintroduced with the same stoichiometric coefficients on the reactant and product sides of the global reaction. The entire balancing process is completely automated in the software.

2.2. Nernst potential and the Nernst equation

Based on the chemical potential balance at open circuit, the Nernst equation provides that:

$$E = E^\circ + \frac{RT}{n_e F}\sum_{k=1}^{K}(v_f' n_{f,k} + v_o' n_{o,k} - v_k'')\ln\left(\frac{p_k}{p_0}\right), \tag{6}$$

where E is the Nernst electric potential, E° the ideal Nernst potential at standard conditions ($p_0 = 1$ atm), p_k the partial pressure of the kth species, T the temperature, $R = 8.314$ J/(mol K) is the universal gas constant, and $F = 96485.309$ C/mol is Faraday's constant. The ideal Nernst potential at the standard conditions is given as:

$$E^\circ = -\frac{\Delta G^\circ}{n_e F}, \tag{7}$$

where ΔG° is the change in standard-state Gibbs free energy between products and reactants of the global reaction Eq. (3). Specifically:

$$\Delta G^\circ = -\sum_{k=1}^{K}(v_f' n_{f,k} + v_o' n_{o,k} - v_k'')\mu_k^\circ, \tag{8}$$

where μ_k° is the standard-state chemical potential of the kth species. The standard-state thermodynamic properties of ideal gases depend on temperature. The needed thermodynamic properties are readily available in databases such as in CHEMKIN [14]. As an alternative to using the species partial pressures, the Nernst equation can also be represented in terms of the species molar concentrations $[X_k]$ as:

$$E = E^\circ + \frac{RT}{n_e F}\sum_{k=1}^{K}(v_f' n_{f,k} + v_o' n_{o,k} - v_k'')\ln[X_k] + \frac{RT}{n_e F}\ln\left(\frac{RT}{p_0}\right)\sum_{k=1}^{K}(v_f' n_{f,k} + v_o' n_{o,k} - v_k''). \tag{9}$$

Fig. 3 illustrates the Nernst potentials for three fuels as a function of fuel utilization (at $T = 750$ °C and $p = 1$ atm). Consider the situation for butane where the global reaction is:

$$C_4H_{10} + \tfrac{13}{2}O_2 \rightarrow 5H_2O + 4CO_2. \tag{10}$$

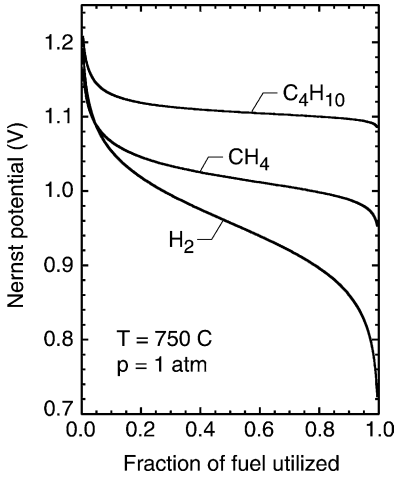

Fig. 3. Nernst potential for three fuels-air systems as a function of percentage of the fuel utilization. As the fuel is "utilized" it is converted to stoichiometric products that dilute the fuel on the anode side. The air is not depleted in this system.

If the fuel is 50% utilized then the fuel mixture is composed of 1/2 moles of C_4H_{10}, 5/2 moles of H_2O, and 4/2 moles of CO_2. The Nernst potentials are highest for the hydrocarbons, assuming direct electrochemical oxidation. The figure also shows that the Nernst potential for hydrogen is reduced most as a function of fuel depletion. The potentials illustrated in Fig. 3 are calculated presuming that the oxidizer is pure air (i.e. no depletion of the oxygen in the air).

2.3. Concentration polarization

For open-circuit conditions (i.e. zero current flow), the species concentrations at the electrolyte interface (three-phase boundary) are the same as those in the bulk channel flow. Denoting the molar species concentrations in the channels as $[X_k]^*$, the Nernst potential is written as:

$$E^* = E^\circ + \frac{RT}{n_e F}\sum_{k=1}^{K}(v_f' n_{f,k} + v_o' n_{o,k} - v_k'')\ln[X_k]^* + \frac{RT}{n_e F}\ln\left(\frac{RT}{p_0}\right)\sum_{k=1}^{K}(v_f' n_{f,k} + v_o' n_{o,k} - v_k''). \tag{11}$$

However, when the current is flowing there must be concentration gradients across the electrode structures. This is because the diffusion processes that supply the species flux to the electrochemical reactions are driven by concentration gradients. Consequently, species concentrations at the three-phase boundaries $[X_k]^s$ are different from the bulk concentrations. Evaluated at the three-phase boundaries, the corresponding Nernst equation is written as:

$$E^s = E^\circ + \frac{RT}{n_e F}\sum_{k=1}^{K}(v_f' n_{f,k} + v_o' n_{o,k} - v_k'')\ln[X_k]^s + \frac{RT}{n_e F}\ln\left(\frac{RT}{P_0}\right)\sum_{k=1}^{K}(v_f' n_{f,k} + v_o' n_{o,k} - v_k''). \tag{12}$$

The potential difference associated with the concentration variation is written in terms of a concentration overpotential as follows:

$$\eta_{\text{conc}} = E^* - E^{\text{s}} = \frac{RT}{n_e F}\sum_{k=1}^{K}(\nu_f' n_{f,k} + \nu_o' n_{o,k} - \nu_{f,k}'' - \nu_{o,k}'')\ln\left(\frac{[X_k]^*}{[X_k]^{\text{s}}}\right). \quad (13)$$

The equation can easily be rewritten to separate the anode and cathode contributions as:

$$\eta_{\text{conc}} = \frac{RT}{n_e F}\sum_{k=1}^{K}(\nu_f' n_{f,k} - \nu_{f,k}'')\ln\left(\frac{[X_k]^*}{[X_k]^{\text{s}}}\right) + \frac{RT}{n_e F}\sum_{k=1}^{K}(\nu_o' n_{o,k} - \nu_{o,k}'')\ln\left(\frac{[X_k]^*}{[X_k]^{\text{s}}}\right). \quad (14)$$

Furthermore, the concentration overpotentials at the anode and the cathode can be defined separately as:

$$\eta_{\text{conc,a}} = \frac{RT}{n_e F}\sum_{k=1}^{K}(\nu_f' n_{f,k} - \nu_{f,k}'')\ln\left(\frac{[X_k]^*}{[X_k]^{\text{s}}}\right), \quad (15)$$

$$\eta_{\text{conc,c}} = \frac{RT}{n_e F}\sum_{k=1}^{K}(\nu_o' n_{o,k} - \nu_{o,k}'')\ln\left(\frac{[X_k]^*}{[X_k]^{\text{s}}}\right). \quad (16)$$

There are a number of physical processes that may contribute to the concentration polarization. These include gas species molecular transport in the electrode pores, solution of reactants into the electrolyte and dissolution of products out of the electrolyte, and the diffusion of the reactants/products through the electrolyte to/from the electrochemical reaction sites. Typically, however, the diffusive transport of the reactants and products between the flow channels and the electrochemical reaction sites across the electrode is the major contributor to the concentration polarization. For an anode-supported MEA structure, the concentration polarization at the cathode is usually very small due to its being very thin (e.g. 50 μm). However, the concentration polarization at the anode can be very significant, particularly at the high current density and high fuel utilization rate.

2.3.1. Dusty-gas model

The concentration polarization is caused primarily by the transport of gaseous species through porous electrodes. It is affected by the microstructure of the electrodes, particularly, the porosity, permeability, pore size, and tortuosity factor. There are four major physical processes that affect transport in the porous media. They are molecular diffusion, Knudsen diffusion, surface diffusion, and Darcy's viscous flow. The relative importance of bulk diffusion (e.g. Fickian) and Knudsen diffusion depends on the relative frequency of molecular-molecular collisions and molecular-wall collisions. These processes can be characterized by the Knudsen number $Kn = \lambda/d$, where λ is the mean free path length in the gas and d is a characteristic pore diameter. When $Kn \ll 1$ bulk diffusion is dominant and when $Kn \gg 1$ Knudsen diffusion is dominant. When $Kn \approx 1$, which is the typical situation in SOFC electrodes, both bulk diffusion and Knudsen diffusion are comparable and must be considered together. The dusty-gas model (DGM) [15] was developed to represent multicomponent transport in this situation.

The dusty-gas model can be used to describe the relationship between the gas species concentrations in the flow channel and concentrations at the electrochemical reaction sites (at the electrode–electrolyte interface). The DGM was developed initially for astrophysical applications, assuming that the pore wall consists of giant, motionless, and uniformly distributed particles (i.e. dust) in space. Three gas-phase transport mechanisms are considered: molecular diffusion, Knudsen diffusion, and viscous flow. Bulk diffusion and Knudsen diffusion are combined in series to form the total diffusive flux. The viscous porous-media flow (Darcy flow) acts in parallel with the diffusive flux. There are three porous-media parameters that appear in the DGM. They are the Knudsen coefficient (K_g), the permeability constant (B_g), and the porosity-to-tortuosity ratio (ϕ_g/τ_g), all which can be determined experimentally. The DGM can be written as an implicit relationship among the molar concentrations, molar fluxes, concentrations gradients, and the pressure gradient [16,17]:

$$\sum_{\ell\neq k}\frac{[X_\ell]N_k^{\text{g}} - [X_k]N_\ell^{\text{g}}}{[X_{\text{T}}]D_{k\ell}^{\text{e}}} + \frac{N_k^{\text{g}}}{D_{k,Kn}^{\text{e}}} = -\nabla[X_k] - \frac{[X_k]}{D_{k,Kn}^{\text{e}}}\frac{B_g}{\mu}\nabla p. \quad (17)$$

In this relationship N_k^{g} is the molar flux of species k, $[X_k]$ the molar concentrations, and $[X_{\text{T}}] = p/RT$ is the total molar concentration. The mixture viscosity is given as μ (which depends on the mixture composition and temperature) and $D_{k\ell}^{\text{e}}$ and $D_{k,Kn}^{\text{e}}$ are the effective molecular binary diffusion coefficients and Knudsen diffusion coefficients.

The effective molecular binary diffusion coefficients in the porous media $D_{k\ell}^{\text{e}}$ are related to the ordinary binary diffusion coefficients $D_{k\ell}$ in the bulk phase [18] as:

$$D_{k\ell}^{\text{e}} = \frac{\phi_g}{\tau_g}D_{k\ell}. \quad (18)$$

Binary diffusion coefficients, which are determined from kinetic theory, may be evaluated with software such as CHEMKIN [18]. Knudsen diffusion, which occurs due to gas–wall collisions, becomes dominant when the mean free path of the molecular species is much larger than the pore diameter. The effective Knudsen diffusion coefficient can be expressed as:

$$D_{k,Kn}^{\text{e}} = \frac{4}{3}K_g\sqrt{\frac{8RT}{\pi W_k}}, \quad (19)$$

where the Knudsen permeability coefficient $K_g = r_p\phi_g/\tau_g$

(ϕ_g is the porosity and τ_g the tortuosity factor), W_k are the molecular weights, and r_p the average pore radius.

Assuming that the porous electrode is formed by closely packed spherical particles with diameter d_p (an idealization), the permeability can be expressed by the Kozeny–Carman relationship as [19]:

$$B_g = \frac{\phi_g^3 d_p^2}{72\tau_g(1-\phi_g)^2}. \tag{20}$$

Other porous-media situations have different permeabilities.

An iterative procedure is needed to determine the pressure and concentration gradients. Assuming that the species molar fluxes N_k^g through the porous electrode are known based on the current density and the global electrochemical reaction at the electrode–electrolyte interface, the pressure gradient can be determined as:

$$-\nabla p = \frac{\sum_k N_k^g / D_{k,Kn}^e}{(1/RT) + (B_g/\mu)\sum_k [X_k]/D_{k,Kn}^e}. \tag{21}$$

This expression for the pressure gradient comes from a summation of Eq. (17) over all species k, recognizing that summation of the first term (representing ordinary diffusion) vanishes exactly. The concentrations $[X_k]$ in the denominator are evaluated either in the channel or at the electrolyte interface, depending on the direction of the net molar flux $\sum_k N_k^g$. If the net flux is toward the electrolyte (as it normally is in the cathode), then the $[X_k]$ are taken as the channel concentrations. However, when the flux is toward the channel (as it usually is in the anode), the concentrations are evaluated at the electrolyte interface. The iteration is needed because the electrolyte interface concentrations are not yet known. Assuming an initial guess for the concentrations $[X_k]$ (usually the channel concentrations), the pressure gradient is evaluated. Then, using this pressure gradient, the concentration gradients can be determined from Eq. (17) as:

$$-\nabla[X_k] = \sum_{\ell \neq k} \frac{[X_\ell]N_k^g - [X_k]N_\ell^g}{[X_T]D_{k\ell}^e} + \frac{N_k^g}{D_{k,Kn}^e} + \frac{[X_k]}{D_{k,Kn}^e}\frac{B_g}{\mu}\nabla p. \tag{22}$$

The concentrations in the summation on the RHS are evaluated as discussed above depending on the direction of the net flux. This analysis is simplified greatly by assuming linear profiles of pressure and concentrations across the electrode. We have justified this assumption by solving the two-dimensional dusty-gas model over a large range of electrode structures and fuel-cell operating conditions. Once the concentration gradients are evaluated, a new estimate for the concentrations at the TPB can be found (assuming linear concentration profiles and a known electrode thickness). With the new estimated concentrations a new pressure gradient can be found. This iteration converges very rapidly—typically needing only two or three iterations.

Assuming a current density i_e and a global electrochemical reaction, the molar flux of the gas species through the anode and cathode can be evaluated as:

$$N_{k,a}^g = (\nu_f{}'_{f,k} - \nu''_{f,k})\frac{i_e}{n_e F}, \tag{23}$$

$$N_{k,c}^g = (\nu_o{}'_{o,k} - \nu''_{o,k})\frac{i_e}{n_e F}. \tag{24}$$

Note that the molar flux must be taken as zero for any inert species that does not participate in the electrochemical reactions (e.g. nitrogen in the cathode). Appendix A provides examples.

2.4. Activation polarization and the Butler–Volmer equation

In the chemical reaction process, the reactants must usually overcome an energy barrier, that is, the activation energy. In charge-transfer electrochemical reactions, the reactants must overcome not only a thermal energy barrier but also an electric potential. Thus, a portion of the potential cell voltage is lost in driving the electrochemical reactions that transfer the electrons to or from the electrodes. This activation polarization is a very important loss when the electrochemical reactions are controlled by the slow electrode kinetics.

Assuming a single rate-controlling reaction, the Butler–Volmer equation [20] provides a relationship between the current density and the charge-transfer overpotential as:

$$i_e = i_0\left[\exp\left(\alpha_a \frac{n_e^{BV} F \eta_{act}}{RT}\right) - \exp\left(-\alpha_c \frac{n_e^{BV} F \eta_{act}}{RT}\right)\right]. \tag{25}$$

This equation represents the net anodic and cathodic current due to an electrochemical reaction. The activation overpotential η_{act} is potential difference above the equilibrium electric potential between the electrode and the electrolyte. The factor n_e^{BV} is the number of electrons transferred in the single elementary rate-limiting step that the Butler–Volmer equation represents. It is quite common to assume $n_e^{BV} = 1$. The anodic and cathodic asymmetric factors (also called charge-transfer coefficients) α_a and α_c determine the relative variations of the anodic and cathodic branches of the total current with an applied overpotential η_{act}. The anodic and cathodic charge-transfer coefficients α_a and α_c depend on the electrocatalytic reaction mechanism and typically take values between zero and one. Further, they are constrained by $\alpha_a + \alpha_c = 1$. The exchange current density i_0 is the current density of the charge-transfer reaction at the dynamic equilibrium electric potential difference E^{eq}. In other words, at the equilibrium potential, the forward and reverse current densities are equal at i_0. A high exchange current density implies the reaction proceeds rapidly upon varying the potential from its equilibrium value. There is an activation overpotential for the anode and the cathode. Consequently, there are charge-transfer coefficients α_a and α_c for both the anode and the cathode.

There are two potentially interesting limits of the Butler–Volmer equation. At very high surface activation overpotential one of the exponential terms in Butler–Volmer equation becomes negligible. The resulting Tafel equation is a straight line on a semi-logarithmic plot, $\ln(i_e) \sim \eta_{act}$. Alternatively stated:

$$\eta_{act} = \frac{RT}{\alpha_a n_e^{BV} F}[\ln(i_e) - \ln(i_0)] \quad \text{for} \quad +\frac{\alpha_a n_e^{BV} F \eta_{act}}{RT} \gg 1, \tag{26}$$

or

$$\eta_{act} = -\frac{RT}{\alpha_c n_e^{BV} F}[\ln(-i_e) - \ln(i_0)] \quad \text{for} \quad -\frac{\alpha_c n_e^{BV} F \eta_{act}}{RT} \gg 1. \tag{27}$$

In an SOFC, the Tafel equation can often be used to calculate the activation overpotential at the cathode. The second limiting case is realized at very lower activation polarization. In this case, the following linear current overpotential relationship applies:

$$\eta_{act} = \frac{RT}{(\alpha_a + \alpha_c) n_e F}\left(\frac{i_e}{i_0}\right). \tag{28}$$

This equation can often be applied to calculate the activation potential at the anode of the SOFC system. In our model neither of these limiting cases is actually used to determine the activation overpotentials. Rather, the Butler–Volmer equation is solved iteratively in its native form.

The exchange current density i_0 is a measure of the electrocatalytic activity of the electrode–electrolyte interface or TPB for a given electrochemical reaction. In fact, the exchange current density is a crucially important factor for determining the activation overpotential η_{act}. However, i_0 is not a simple constant parameter, but its value may depend on the operating conditions and material properties, including concentrations of reactants and products adjacent to the electrode, temperature, pressure, the microstructure and electrocatalytic activity of the electrode, and even the conductivity of the electrolyte [21]. Particularly for composite SOFC electrodes with the mixed ionic and electronic conduction, such as a Ni–YSZ for the anode and a LSM–YSZ for the cathode, the electrochemical reaction zone can be extended from the electrolyte-electrode interface into the electrode. Thus, the charge-transfer resistance can be reduced and the exchange current density can be enhanced. Furthermore, the exchange current density for the composite electrode becomes a function of the electrochemical properties of the electrolyte and electrode and the effective TPB length. Thus, microstructural properties of the composite electrode, such as the grain size and volume fraction of the electrolyte, will affect the exchange current density. A steady-state current–voltage experiment can measure i_0 at a particular operating condition. However, it is very difficult to obtain a general analytical expression for i_0, which requires detailed understanding of the elementary thermal and electrochemical reaction mechanisms occurring at the electrode and the microstructure of the electrode.

In our model we provide flexibility for the exchange current density to depend on the reactant concentrations as:

$$i_0 = i_0^0 \prod_{k=1}^{K} X_k^{\gamma_k}, \tag{29}$$

where i_0^0 is a constant and γ_k and X_k the reaction order and mole fraction (at the electrode–electrolyte interface) for the kth species, respectively. Although this formulation provides flexibility in the model, it is still far from a general description of the elementary charge-transfer reactions steps. Furthermore, it is difficult to determine the reaction orders for any particular system.

At the cathode of an SOFC system, the gas-phase oxygen reduction and ion incorporation into the electrolyte is a complex process that involves a series of elementary reactions steps, including the oxygen adsorption and dissociation on the surface, diffusion of the intermediate species on the surface, charge transfer, and oxygen incorporation into the lattice of the electrolyte. Any of the reaction steps may be the rate-limiting reaction for the overall process, depending on the operating conditions (temperature, oxygen partial pressure), and material properties, and microstructure of the electrode (catalytic activity, pore size, porosity, tortuosity, and permeability). For the LSM–YSZ composite cathode, Kim et al. [22] have indicated that: (1) $i_0 \sim p_{O_2}^{3/8}$ if the rate-determining step is the charging step of adsorbed oxygen; (2) $i_0 \sim p_{O_2}^{1/4}$ if the rate-determining step is diffusion of charged surface oxygen to the TPB; and (3) i_0 does not depend on p_{O_2} if the rate-determining step is incorporation of oxygen ions into the electrolyte. For the Pt–YSZ cathode, the exchange current density i_0 was shown to be proportional to $p_{O_2}^{1/4}$ at low p_{O_2} and $p_{O_2}^{-1/4}$ at high p_{O_2} [23]. Uchida et al. [21] indicated that i_0 may be proportional to the ionic conductivity of the electrolyte for both the LSM–YSZ and Pt–YSZ cathodes depending on the operating temperatures.

The situation is more complex at the anode of an SOFC system. Reaction of a hydrocarbon fuel may involve direct electrochemical oxidization [24], steam and/or dry reforming, pyrolysis, and deposit formation. The general thermal and electrochemical reaction steps may include dissociative adsorption on surfaces, surface and/or charge-transfer reactions among the adsorbed intermediate species, surface and/or bulk diffusion of the adsorbed species, and desorption of products. Even for hydrogen, the simplest and most widely studied fuel, there is still considerable debate about the underlying electrochemical processes [5,7,25–27]. The rate-determining reaction step of the hydrogen oxidation at the anode may be the dissociative adsorption of hydrogen, the formation of hydroxyl, a charge-transfer

reaction, or the desorption of water, all of which can depend on the operating conditions (such as the temperature, pressure, and species concentrations), macro- and microstructures, and material properties of the electrode. Additionally thermal and electrochemical reactions may occur on the surface and in the bulk of the metal and/or ceramic of the composite cermet electrode. Thus, there is not a simple means to represent the relationship between the exchange current density and the species concentrations at the anode.

There are ways to measure the exchange current density (or infer its value from related measurements). Based on the Butler–Volmer equation, a charge-transfer resistance R_{ct} can be expressed as:

$$R_{ct}^{-1} = A_{tpb}\left(\frac{\partial i_e}{\partial \eta}\right)_{[X_k],T} = i_0 A_{tpb}\frac{n_e^{BV}F}{RT}\left[\alpha_a \exp\left(\alpha_a \frac{n_e^{BV}F\eta}{RT}\right) + \alpha_c \exp\left(-\alpha_c \frac{n_e^{BV}F\eta}{RT}\right)\right]. \quad (30)$$

At the zero activation overpotential:

$$R_{ct} = \frac{RT}{i_0 A_{tpb}(\alpha_a + \alpha_c) n_e^{BV} F}, \quad (31)$$

which presents a relationship between the exchange current density i_0 and the charge-transfer resistance R_{ct}. The charge-transfer resistance can be determined from EIS measurements [6,13].

2.5. Ohmic polarization

Sources of ohmic losses in a fuel cell are the resistance to the ion flow in the electrolyte and the resistance to the electronic flow in the electrode. Due to typically high metal loading resistive electric conductivity in the electrodes is high, which limits ohmic losses in the electrodes. Thus, ohmic polarization in an SOFC system is typically dominated by ion resistance through the electrolyte. Such losses can be reduced by decreasing the electrolyte thickness and enhancing its ionic conductivity.

Since electric current flow in the electrolyte and electrodes obey Ohm's law, the ohmic losses can be expressed simply as:

$$\eta_{ohm} = i_e R_{tot}, \quad (32)$$

where R_{tot} is the total area-specific cell resistance, including the area-specific resistances in the electrode R_{ed} and the solid electrolyte R_{el}. The ionic conductivity of the electrolyte can usually expressed as:

$$\sigma_{el} = \sigma_0 T^{-1} \exp\left(-\frac{E_{el}}{RT}\right), \quad (33)$$

where E_{el} is the activation energy for the ionic transport. Thus, the specific ohmic resistance of the electrolyte with thickness of L_{el} can be obtained as:

$$R_{el} = \frac{L_{el}}{\sigma_{el}}. \quad (34)$$

There are several opportunities for interface overpotentials with in the MEA structure. For example, anywhere two materials are physically bonded together there can be a resistance the causes an interface overpotential, $\eta_{interface}$.

If the electrolyte has electrical conductivity, there is a possibility for a leakage current that may be represented as a leakage overpotential $\eta_{leakage}$. In our model:

$$\eta_{leakage} = \eta^0_{leakage}\left(1 - \frac{i}{i_{max}}\right), \quad (35)$$

where $\eta^0_{leakage}$ is the leakage overpotential at open circuit and i_{max} the maximum current density for the cell. Once the Nernst potential is known, $\eta^0_{leakage}$ can be observed from measurement of the open-circuit potential. The value of i_{max} can be determined from the model by calculating current density at which the cell power density vanishes.

3. Solution algorithm

The model is "solved" by determining the cell voltage for a given current density, or vice versa. In general, the cell potential E_{cell} is expressed as the difference between the Nernst cell potential E and the sum of all the relevant overpotentials, which depend on current density (Eq. (1)). For a given cell configuration, with specified geometry and material properties, as well as operating conditions (e.g. pressure, temperature, and fuel and oxidizer composition), each of the overpotentials must be evaluated as a function of current density. Since the overpotential is usually an implicit function of current density an iteration is needed. Most of the iterations are accomplished using a Newton–Raphson method. The solution procedure follows several steps as follows:

- Calculate the stoichiometric coefficients of the global electrochemical reaction by solving element balance equations. This depends on the specific fuel and oxidizer composition.
- Based on the stoichiometric coefficients, evaluate the charge transferred n_e and the Nernst potential E.
- Evaluate the species molar flux through the anode and the cathode ($N^g_{a,k}$ and $N^g_{c,k}$). These are all evaluated explicitly from the current density and the stoichiometry (Eqs. (23) and (24)).
- Calculate the species compositions at the electrode–electrolyte interfaces ($[X_k]^s$) from the DGM at given species molar flux and species compositions in the channels. This is an iterative procedure.
- Evaluate the concentration overpotentials for both electrodes ($\eta_{conc,a}$ and $\eta_{conc,c}$) once the interface concentra-

tions are known (Eqs. (15) and (16)). This is an explicit evaluation.

- With a specified exchange current density i_0 at the anode and cathode, invert the Butler–Volmer equation to obtain the activation overpotentials $\eta_{act,a}$ and $\eta_{act,c}$. This is an iterative procedure.
- Calculate the ohmic overpotential η_{ohm} in the electrolyte (Eq. (32)). This is an explicit procedure.
- Determine the leakage overpotential $\eta_{leakage}$ (Eq. (35)). Assuming that $\eta^0_{leakage}$ is specified, the value of i_{max} must be determined iteratively. The maximum current density is achieved when the net voltage is zero. The value of i_{max} depends on the cell parameters as well as all the other overpotentials. For a given current density i_e, evaluate the leakage overpotential.
- With all the overpotentials in hand, evaluate the cell voltage E_{cell}.

The procedure described above assumes that the cell voltage is to be determined once a current density is specified. To create a voltage–current plot, for example, the procedure is repeated for a range of current densities. When the MEA model is incorporated into a larger system-level fuel-cell model, it is usually more natural to specify the cell operating voltage and determine the local current density. In this case an outer iteration is implemented around the whole procedure outlined above. Despite the nested iterations, the convergence is very rapid.

4. Analysis of a methane-fueled SOFC

The objective of this section is to apply the model to a particular anode-supported SOFC system operating with methane as the fuel. Table 1 lists model parameters of the unit cell. For an anode-supported SOFC system, both the electrolyte and the cathode are much thinner than the anode. Thus, it may be anticipated that the electrolyte, ohmic and cathode-concentration overpotentials will be relatively small. The transport parameters for calculating the ohmic overpotentials in the electrolyte (Table 1) are based on the oxygen-vacancy conductivity [28].

Assuming pure CH_4 as a fuel and air as the oxidizer, Fig. 4 illustrates the predicted cell voltage and the power density as a function of the current density. The peak power is seen to be about 0.4 W/cm^2 at about 0.4 V. Fig. 4 also shows the contributions of all the overpotentials as shaded regions. For this particular system, the cathode activation represents the largest overpotential. It is followed by the anode-activation, ohmic, and anode-concentration overpotentials. The cathode-concentration overpotential is so small that it does not show on the plot. All the overpotentials increase with increasing current density. The sum of the overpotentials reaches the Nernst potential (in this case, about 1.15 V) at the highest current density ($i_e \approx 2.25$ A/cm^2) where the power is reduced to zero. In other words, the cell ceases to produce power when the overpotentials just equal the cell potential.

Table 1
Parameters to represent a CH_4 SOFC system

Parameter	Value
Operating temperature (T, °C)	750
Operating pressure (p, atm)	1
Anode	
Thickness (L_a, μm)	1000
Porosity (ϕ_g)	0.35
Tortuosity (τ_g)	3.50
Average pore radius (r_p, μm)	1
Average particle diameter (d_p, μm)	10
Exchange current density (i_0, A/cm^2)	0.40
Charge-transfer coefficient (α_a)	0.50
Number of electrons (n_e^{BV})	1
Cathode	
Thickness (L_c, μm)	50
Porosity (ϕ_g)	0.35
Tortuosity (τ_g)	3.50
Average pore radius (r_p, μm)	1
Average particle diameter (d_p, μm)	10
Exchange current density (i_0, A/cm^2)	0.13
Charge-transfer coefficient (α_a)	0.50
Number of electrons (n_e^{BV})	1
Electrolyte	
Thickness (L_{el}, μm)	20
Activation energy of O^{2-} (E_{el}, J/mol)	8.0E+4
Pre-factor of O^{2-} (σ_0, S/cm)	3.6E+5
Leakage overpotential (η_{max}, V)	0.0

4.0.1. Fuel utilization

Because fuel is consumed by electrochemical reaction as it flows through the anode channel, the fuel stream is diluted by product species (CO_2 and H_2O). Furthermore, as fuel is

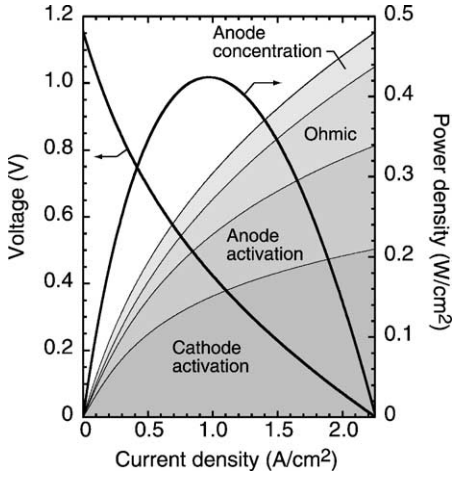

Fig. 4. Cell voltage, overpotentials, and power density as a function of the current density for CH_4 as a fuel in an SOFC with parameters stated in Table 1.

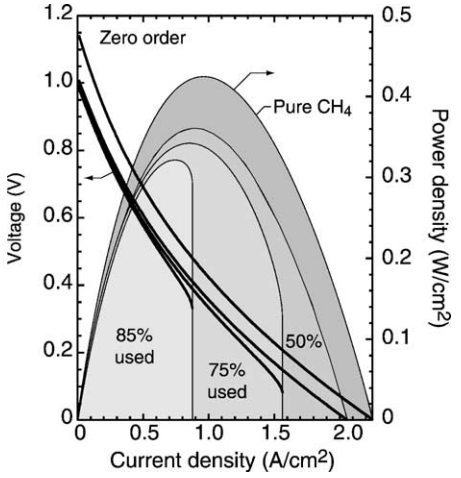

Fig. 5. Cell voltages and power densities as a function of the current density for fuel CH_4 at a different percentage of fuel utilization. The exchange current density is set to be constant.

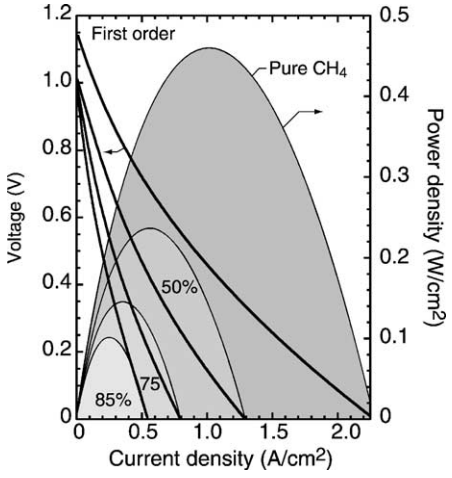

Fig. 6. Cell voltages and power densities as a function of the current density for CH_4 at a different percentage of fuel utilization. The exchange current density is assumed to be the first order in the fuel concentration.

used, the Nernst potential decreases (Fig. 3). The various overpotentials are also affected by the fuel depletion. Fig. 5 illustrates the cell performance for situations where the fuel is 50, 75, and 85% used. In this example, the exchange current densities i_0 at the anode and cathode are set to be constants (Table 1). Furthermore, the cathode channel is presumed to be pure air (i.e. no oxygen depletion). At 75 and 85% fuel utilization there are seen to be critical current densities at which the power abruptly terminates. In these cases (approximately 1.57 A/cm^2 for the 75% case and approximately 0.88 A/cm^2 for the 85% case), the anode-concentration overpotential becomes so large that no fuel can reach the anode three-phase boundary. As a result the cell cannot operate.

The cell represented by Fig. 5 would operate well at very high fuel utilization. For example, if the operating voltage was set at 0.5 V the current density would vary relatively little (approximately between 0.6 and 0.8 A/cm^2) with corresponding variations in power density (approximately between 0.42 and 0.32 W/cm^2) as the composition in the fuel channel varies between pure methane and a highly diluted stream where the fuel is 85% depleted.

Fig. 6 presents the result of another simulation where all parameters except one are the same as for the simulation shown in Fig. 5. The cell represented by Fig. 6 presumes that the anode exchange current density is first order in the fuel concentration. That is:

$$i_0 = i_0^0 X_{CH_4}, \tag{36}$$

where X_{CH_4} is the fuel mole fraction and $i_0^0 = 0.65$ A/cm^2. As the fuel is depleted, the exchange current density drops proportionally. In this case, the results are strikingly different. As the fuel is depleted the current density and the power density are significantly diminished. The anode-activation overpotential dominates the losses. It would likely be impractical to operate such a cell at a fuel utilization greater than about 50%.

5. Interpreting experimental observations

Gorte et al. [1,24] have measured SOFC performance for a variety of fuels using a YSZ electrolyte and a Cu–ceria–YSZ cermet anode. Fig. 7 reproduces some of the reported measurements together with results from our model.

Table 2 lists parameters used in our MEA model to fit the experimental data for the case of H_2 as the fuel. Some of the physical and operating parameters are reported [1,24], but we have estimated others. The parameters at the cathode are chosen such that the concentration overpotential is very small. The transport parameters for calculating the

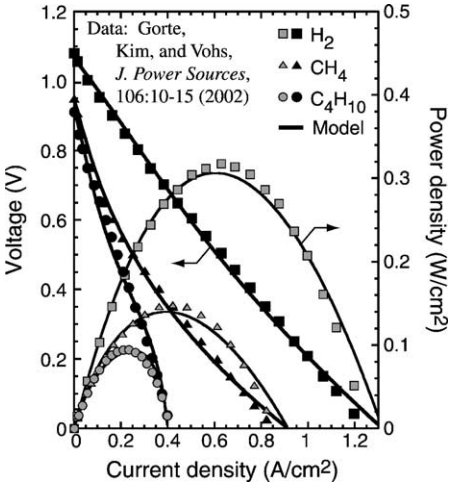

Fig. 7. The MEA model is used to represent a range of experimental data of current–voltage and power densities for an SOFC from Gorte et al. [1,24] by varying a few parameters.

Table 2
Parameters for matching the H_2 experimental data by Gorte et al. [1,24]

Parameter	Value
Operating temperature (T, °C)	700
Operating pressure (p, atm)	1
Anode (Cu–ceria–YSZ)	
Thickness (L_a, μm)	400
Porosity (ϕ_g)	0.52
Tortuosity (τ_g)	3.50
Average pore radius (r_p, μm)	1.0
Average particle diameter (d_p, μm)	3.0
Exchange current density (i_0^0, A/cm^2)	0.0055
Charge-transfer coefficient (α_a)	0.50
Number of electrons (n_e)	1
Cathode (LSM–YSZ)	
Thickness (L_c, μm)	50
Porosity (ϕ_g)	0.35
Tortuosity (τ_g)	3.50
Average pore radius (r_p, μm)	1.0
Average particle diameter (d_p, μm)	3.0
Exchange current density (i_0^0, A/cm^2)	0.75
Reaction order of O_2	0.5
Charge-transfer coefficient (α_a)	0.5
Number of electrons (n_e)	1
Electrolyte (YSZ)	
Thickness (L_{el}, μm)	60
Activation energy of O^{2-} (E_{el}, J/mol)	8.0E+4
Pre-factor of O^{2-} (σ_0, S/cm)	3.6E+5
Leakage overpotential (η_{max}, V)	0.07

ohmic overpotentials in the electrolyte are based on the oxygen-vacancy conductivity of YSZ [28]. To match the experimental data for cases of CH_4 and C_4H_{10}, the parameters: porosity, exchange current density, reaction orders and the leakage overpotential are adjusted as indicated in Table 3.

As illustrated in Fig. 7, the experimental measurements can be represented very well by our model through varying a few parameters. We must hasten to caution, however, that we claim no uniqueness in the set of parameters used. Moreover, although the model can match the data, it is difficult to support some of the "best-fit" parameters on physical grounds. Nevertheless, we believe that one can gain valuable insights through interpreting experimental observations in the context of a quantitative, physically based model.

As shown in Fig. 7, the measured open-circuit cell potential for the H_2 case is very close to the theoretical Nernst potential. However, for the CH_4 and C_4H_{10} cases the measured open-circuit potentials are approximately 0.2 V lower than the corresponding theoretical Nernst potentials. Therefore, we have assigned a leakage overpotential to capture the measured open-circuit potential (Table 3).

Close inspection reveals that the current–voltage curves for these three fuels have substantially different functional forms. The varying shapes infer that the overpotential losses for these three fuels are dominated by different physico-chemical processes. For the H_2 fuel, the nearly straight-line shape (for the entire range of current densities), indicates that the major polarization may be due to the ohmic loss at the electrolyte rather than the activation overpotential and concentration overpotential at the anode. For CH_4, the data shows a substantial upward curvature at low current density but a nearly linear function at high current density. In this case, the major overpotential loss may be caused by the relatively low anode activation. In the case of C_4H_{10}, the current–voltage curve is again functionally different from the other fuels, particularly at the high current density. The relatively lower power density indicates that the activation overpotential is very important, and the downward curvature at the high current density indicates a significant anode-concentration overpotential.

Since the concentration overpotentials appear to be relatively small for cases of H_2 and CH_4, we have used the measured values for porosity and pore size. In these cases, we have varied the exchange current densities and reaction orders to fit these measurements. However, for the case of C_4H_{10} fuel, the anode-concentration overpotential appears to dominate the potential losses, particularly at the high current density. Consequently, it appears that the gas-transport resistance through the anode must be increased. The most direct way to increase transport resistance is to reduce the anode porosity. A very low porosity of $\phi \approx 2\%$ is needed to reproduce the observed strong curvature in the data. Since the measured porosity is $\phi \approx 50\%$, one must seriously question the physical validity of the porosity needed to fit the data. It is more likely that there may be some important physical process that is not represented in the model as it currently stands. For example, is it possible that there is significant catalytic reaction within the anode structure? If so, perhaps it is not the parent butane fuel that reacts electrochemically, but rather some reaction products. Certainly if one of the essential underpinnings of the model (e.g. direct electrochemical oxidation of the fuel) is incorrect, then inferences from the data-fitting procedure must be questioned.

Table 3
Parameters adjusted to match the experiment data by Gorte et al. [1,24]

Fuel type	Reaction order (γ_k)					ϕ	i_0^0 (A/cm^2)	$\eta_{leakage}^0$ (V)
	H_2	CH_4	C_4H_{10}	H_2O	CO_2			
Hydrogen (H_2)	1.0	0.0	0.0	−1.0	0.0	0.520	0.0055	0.07
Methane (CH_4)	0.0	1.0	0.0	−0.5	0.0	0.520	0.0045	0.20
Butane (C_4H_{10})	0.0	0.0	1.0	−1.0	0.0	0.021	0.0090	0.23

6. Summary and conclusions

We have presented a physically based mathematical model that represents a unit cell of a fuel-cell membrane-electrode assembly. It is written to accommodate general descriptions of fuel and oxidizer mixtures. It considers a variety of anode and cathode overpotential losses that include activation, concentration, ohmic, and leakage. The activation overpotentials are described in terms of the Butler–Volmer equation. Concentration overpotentials in the porous electrode structures are described in terms of a dusty-gas model. Ohmic losses may stem from ion resistance in the electrolyte or electrical resistance at material interfaces.

The model can be exercised to produce voltage–current relationships for a certain cell configurations and specified operating conditions. These simulations are valuable in helping to understand the competing physical processes that are responsible for controlling cell performance. Such understanding can assist in cell design and optimization as well as interpreting experimental observations.

The objective of this paper is primarily to describe the MEA model and the underlying assumptions. The model can be used as a stand-alone model. However, the software is written to be incorporated as a submodel into larger system-level models that also consider the fluid flow and thermal transport for a full fuel-cell system.

The model presented here assumes direct electrochemical oxidation of the fuel species. Thus, while there is multi-component transport of fuel, oxidizer, and product species within the electrode structures, there is no homogeneous or catalytic reaction among these species. Although there is reported experimental evidence of DECO [24] for hydrocarbon fuels in certain SOFC systems, there is also reason to anticipate that catalytic reaction could occur within porous cermet electrode structures. Thus, in future work we intend to extend the models to accommodate this possibility.

Acknowledgements

This work has been supported by DAPRA through the Palm Power program and by the DoD Multidisciplinary University Research Initiative (MURI) program administered by the Office of Naval Research under Grant N00014-02-1-0665. We gratefully acknowledge frequent and substantial collaboration with Prof. Greg Jackson (University of Maryland) and Prof. David Goodwin (Caltech). We also acknowledge close and beneficial collaborations with graduate student Kevin Walters and colleagues at ITN Energy Systems, especially Neal Sullivan and Bill Barker.

Appendix A

This paper develops and discusses a general formalism beginning with a global electrochemical reaction for direct electrochemical oxidation. To maintain generality there is a certain level of abstract nomenclature that must be used. The objective of this appendix is to assist understanding and interpreting the nomenclature by working through specific examples.

A.1. C_4H_{10}–air SOFC

The overall electrochemical reaction is stated as:

$$\mathrm{C_4H_{10}} + \frac{13}{2\times 0.21}(0.21\mathrm{O_2} + 0.79\mathrm{N_2}) \rightarrow 4\mathrm{CO_2} + 5\mathrm{H_2O} + \frac{13\times 0.79}{2\times 0.21}\mathrm{N_2}, \tag{A.1}$$

which combines the electrochemical reaction in the anode:

$$\mathrm{C_4H_{10}} + 13\mathrm{O^{2-}} \rightarrow 4\mathrm{CO_2} + 5\mathrm{H_2O} + 26\mathrm{e^-}, \tag{A.2}$$

and the electrochemical reaction in the cathode:

$$\tfrac{13}{2}\mathrm{O_2} + 26\mathrm{e^-} \rightarrow 13\mathrm{O^{2-}}. \tag{A.3}$$

The fuel and oxidizer compositions are specified by setting the non-zero $n_{\mathrm{f},k}$ and $n_{\mathrm{o},k}$ as:

$$n_{\mathrm{f,C_4H_{10}}} = 1, \tag{A.4}$$

$$n_{\mathrm{o,O_2}} = 0.21, \qquad n_{\mathrm{o,N_2}} = 0.79. \tag{A.5}$$

Balancing the reaction yields the non-zero stoichiometric coefficients as:

$$\nu_{\mathrm{f}}' = 1, \tag{A.6}$$

$$\nu_{\mathrm{o}}' = \frac{13}{2\times 0.21}, \tag{A.7}$$

$$\nu''_{\mathrm{f,CO_2}} = 4, \qquad \nu''_{\mathrm{f,H_2}O} = 5, \tag{A.8}$$

$$\nu''_{\mathrm{o,N_2}} = \frac{13\times 0.79}{2\times 0.21}. \tag{A.9}$$

The non-zero charge transfer per mole of each reactant species are:

$$z_{\mathrm{f,CH_4}} = 26, \qquad z_{\mathrm{o,O_2}} = 4. \tag{A.10}$$

With the reaction balanced and the charge transfers assigned, the number of electrons transferred by the global reaction follows from Eq. (4) as:

$$n_{\mathrm{e}} = \sum_{k=1}^{K} \nu_{\mathrm{f}}' n_{\mathrm{f},k} z_{\mathrm{f},k} = 26. \tag{A.11}$$

The concentration overpotentials are expressed as:

$$\eta_{\mathrm{conc,a}} = \frac{RT}{26F}\left(\ln\left(\frac{[\mathrm{C_4H_{10}}]^*}{[\mathrm{C_4H_{10}}]^{\mathrm{s}}}\right) - 4\ln\left(\frac{[\mathrm{CO_2}]^*}{[\mathrm{CO_2}]^{\mathrm{s}}}\right) - 5\ln\left(\frac{[\mathrm{H_2O}]^*}{[\mathrm{H_2O}]^{\mathrm{s}}}\right)\right), \tag{A.12}$$

$$\eta_{\mathrm{conc,c}} = \frac{RT}{4F}\ln\left(\frac{[\mathrm{O_2}]^*}{[\mathrm{O_2}]^{\mathrm{s}}}\right). \tag{A.13}$$

For the butane–air case, the species molar fluxes in the anode are:

$$N^{g}_{C_4H_{10}} = \frac{i_e}{26F}, \qquad N^{g}_{H_2O} = -\frac{5i_e}{4F}, \qquad N^{g}_{CO_2} = -\frac{4i_e}{8F}, \tag{A.14}$$

and in the cathode are:

$$N^{g}_{O_2} = \frac{i_e}{4F}, \qquad N^{g}_{N_2} = 0. \tag{A.15}$$

A.2. Fuel-mixture–air SOFC

This example considers the anode channel to have a mixture of fuel (CH_4), products (H_2O and CO_2), and oxygen (O_2). At some particular point in the fuel-cell system the mole ratios in the anode channel are presumed to be CH_4:H_2O:CO_2:O_2=1.0:0.3:0.15:0.05.

This oxygen is explicitly added to the anode stream—it is not coming through the MEA. The oxidizer is presumed to be air. The overall electrochemical reaction can be represented as follows:

$$\begin{aligned}&(CH_4 + 0.3H_2O + 0.15CO_2 + 0.05O_2)\\ &\quad + \tfrac{2}{0.21}(0.21O_2 + 0.79N_2)\\ &\rightarrow (2.3H_2O + 1.15CO_2 + 0.05O_2) + (\tfrac{2}{0.21})0.79N_2.\end{aligned} \tag{A.16}$$

The half-cell reactions combine the electrochemical reaction in the anode:

$$CH_4 + 4O^{2-} \rightarrow CO_2 + 2H_2O + 8e^-, \tag{A.17}$$

and the electrochemical reaction in the cathode:

$$2O_2 + 8e^- \rightarrow 4O^{2-}. \tag{A.18}$$

The fuel and oxidizer compositions are specified by setting the non-zero $n_{f,k}$ and $n_{o,k}$ as:

$$n_{f,CH_4} = 1, \qquad n_{f,H_2O} = 0.3, \qquad n_{f,CO_2} = 0.15, \qquad n_{f,O_2} = 0.05, \tag{A.19}$$

$$n_{o,O_2} = 0.21, \qquad n_{o,N_2} = 0.79. \tag{A.20}$$

Balancing the reaction yields the non-zero stoichiometric coefficients as:

$$\nu_f' = 1, \qquad \nu_o' = \tfrac{2}{0.21}, \tag{A.21}$$

$$\nu''_{f,CO_2} = 1.15, \qquad \nu_{f,H_2}O'' = 2.3, \qquad \nu''_{f,O_2} = 0.05, \qquad \nu''_{o,N_2} = \frac{2 \times 0.79}{0.21}. \tag{A.22}$$

The non-zero charge transfer per mole of each reactant species are:

$$z_{f,CH_4} = 8, \qquad z_{o,O_2} = 4. \tag{A.23}$$

With the reaction balanced and the charge transfers assigned, the number of electrons transferred by the global reaction follows from Eq. (4) as:

$$n_e = \sum_{k=1}^{K} \nu_f' n_{f,k} z_{f,k} = 8. \tag{A.24}$$

The concentration polarizations at the anode and cathode are expressed as:

$$\eta_{conc,a} = \frac{RT}{8F}\left(\ln\left(\frac{[CH_4]^*}{[CH_4]^s}\right) - \ln\left(\frac{[CO_2]^*}{[CO_2]^s}\right) - 2\ln\left(\frac{[H_2O]^*}{[H_2O]^s}\right)\right), \tag{A.25}$$

$$\eta_{conc,c} = \frac{RT}{4F}\ln\left(\frac{[O_2]^*}{[O_2]^s}\right). \tag{A.26}$$

The species molar fluxes in the anode are:

$$N^{g}_{CH_4} = \frac{i_e}{8F}, \qquad N^{g}_{H_2O} = -\frac{i_e}{4F}, \qquad N^{g}_{CO_2} = -\frac{i_e}{8F}, \qquad N^{g}_{O_2} = 0, \tag{A.27}$$

and in the cathode are:

$$N^{g}_{O_2} = \frac{i_e}{4F}, \qquad N^{g}_{N_2} = 0. \tag{A.28}$$

References

[1] R.J. Gorte, S. Park, J.M. Vohs, C. Wan, Anodes for direct oxidation of dry hydrocarbons in a solid-oxide fuel cell, Adv. Mater. 12 (2000) 1465–1469.

[2] E.P. Murray, T. Tsai, S.A. Barnett, A direct-methane fuel cell with a ceria-based anode, Nature 400 (1999) 651–659.

[3] S. Park, J.M. Vohs, R.J. Gorte, Direct oxidation of hydrocarbons in a solid-oxide fuel cell, Nature 404 (2000) 265–266.

[4] C. Wang, W.L. Worrell, S. Park, J.M. Vohs, R.J. Gorte, Fabrication and performance of thin-film YSZ solid oxide fuel cells, J. Electrochem. Soc. 148 (2001) 864–868.

[5] A. Bjeberle, The electrochemistry of solid oxide fuel cell anodes: experiments, modeling, and simulations, Ph.D. thesis, Swiss Federal Institute of Technology, Zürich, 2000.

[6] A. Mitterdorfer, Identification of the oxygen reduction at cathodes of solid oxide fuel cells, Ph.D. thesis, Swiss Federal Institute of Technology, Zürich, 1997.

[7] A.S. Ioselevich, A.A. Kornyshev, Phenomenological theory of solid oxide fuel cell anode, Fuel Cells 1 (2001) 40–65.

[8] S.H. Chan, K.A. Khor, Z.T. Xia, A complete polarization model of a solid oxide fuel cell and its sensitivity to the change of cell component thickness, J. Power Sources 93 (2001) 130–140.

[9] J.W. Kim, A.V. Virkar, K.Z. Fung, K. Mehta, S.C. Singhal, Polarization effects in intermediate temperature, anode-supported solid oxide fuel cells, J. Electrochem. Soc. 146 (1999) 69–78.

[10] A.V. Virkar, J.Chen, C.W. Tanner, J.W. Kim, The role of electrode microstructure on activation and concentration polarizations in solid oxide fuel cells, Solid State Ionics 131 (2000) 189–198.

[11] C.W. Tanner, K.Z. Fung, A.V. Virkar, The effect of porous composite electrode structure on solid oxide fuel cell performance, I. Theoretical analysis, J. Electrochem. Soc. 144 (1997) 21–30.

[12] S.B. Adler, J.A. Lane, B.C.H. Steele, Electrode kinetics of porous mixed-conducting oxygen electrodes, J. Electrochem. Soc. 143 (1996) 3554–3564.

[13] J.R. Macdonald, Impedance Spectroscopy: Emphasizing Solid Materials and Systems, Wiley, New York, 1987.
[14] R.J. Kee, F. Rupley, J.A. Miller, The CHEMKIN thermodynamic database, Technical Report SAND87-8215, Sandia National Laboratories, 1987.
[15] E.A. Mason, A.P. Malinauskas, Gas Transport in Porous Media: The Dusty-Gas Model, Elsevier, New York, 1983.
[16] T. Thampan, S. Malhotra, H. Tang, R. Datta, Modeling of conductive transport in proton-exchange membranes for fuel cell, J. Electrochem. Soc. 147 (2000) 3242–3250.
[17] T. Thampan, S. Malhotra, J. Zhang, R. Datta, PEM fuel cell as a membrane reactor, Catal. Today 67 (2001) 15–32.
[18] R.J. Kee, G. Dixon-Lewis, J. Warnatz, M.E. Coltrin, J.A. Miller, A Fortran computer code package for the evaluation of gas-phase multicomponent transport properties, Technical Report SAND 86-8246, Sandia National Laboratories, 1986.
[19] J. Bear, Dynamics of Fluids in Porous Media, Elsevier, New York, 1972.
[20] A.J. Bard, L.R. Faulkner, Electrochemical Methods: Fundamentals and Applications, 2nd ed., Wiley, New York, 2000.
[21] H. Uchida, M. Yoshida, M. Watanabe, Effect of ionic conductivity of zirconia electrolytes on the polarization behavior of various cathodes in solid fuel cells, J. Electrochem. Soc. 146 (1999) 1–7.
[22] J.D. Kim, G.D. Kim, J.W. Moon, Y. Park, W.H. Lee, KI. Kobayashi, M. Nagai, C.E. Kim, Characterization of LSM–YSZ composite electrode by ac impedance spectroscopy, Solid State Ionics 143 (2001) 379–389.
[23] C.G. Vayenas, S.I. Bebelis, I.V. Yentekakis, S.N. Neophytides, Electrocatalysis and electrochemical reactors, in: P.J. Gellings, H.J.M. Bouwmeester (Eds.), The CRC Handbook: Solid State Electrochemistry, CRC Press, Boca Raton, 1997, pp. 445–480.
[24] R.J. Gorte, H. Kim, J.M. Vohs, Novel SOFC andoes for the direct electrochemical oxidation of hydrocarbon, J. Power Sources 106 (2002) 10–15.
[25] B. de Boer, SOFC anode: hydrogen oxidation at porous nickel and nickel/yttria-stabilised zirconia cermet electrodes, Ph.D. thesis, University of Twente, The Netherlands, 1998.
[26] M. Ihara, T. Kusano, C. Yokoyama, Competitive adsorption reaction mechanism of Ni/yttria-stabilized zirconia cermet anodes in H_2–H_2O solid oxide fuel cells, J. Electrochem. Soc. 148 (2001) A209–A219.
[27] X. Wang, N. Nakagawa, K. Kato, Anodic polarization related to the ionic conductivity of zirconia at Ni–zirconia/zirconia electrodes, J. Electrochem. Soc. 148 (2001) A565–A569.
[28] K. Sasaki, J. Maier, Re-analysis of defect equilibria and transport parameters in Y_2O_3-stabilized ZrO_2 using EPR and optical relaxation, Solid State Ionics 134 (2000) 303–321.